Supplementary material

Self-propelled Two Dimensional Polymer Multilayer Plate Micromotors

Meiyu Gai[1,2], Johannes Frueh*[1], Narisu Hu[1], Tieyan Si[1], Gleb Sukhorukov[2], Qiang He*[1]

[1]Key Laboratory of Microsystems and Microstructures Manufacturing, Ministry of Education, Micro/Nano Technology Research Centre, Harbin Institute of Technology, Yikuang Street 2, Harbin 150080, China

[2] Queen Mary University of London, Mile End, Eng, 215, London E1 4NS, United Kingdom

Overview of existing methods for motion description of bubble propelled colloidal particles

The movement mechanism of colloidal particles can be switched from diffusophoresis to bubble propulsion depending on the particle composition (e.g. using 2 different metals on different particle areas), roughness, hydrogen peroxide concentration and the nucleation site availability.[1] In an earlier publication, the moving speed of colloidal particles was connected to the hydrogen peroxide concentration as well as surface tension, temperature and bubble size.[2] One must note that the maximum modeled speed in that publication was 5-6 μm/S in 8% hydrogen peroxide.[2] This speed is much lower than experimental results for similar particle size, composition and hydrogen peroxide concentrations, reaching up to 200 μm/S.[3]

A report that SDS (sodium dodecyl sulphate) decreases the colloidal motor speed is in strong contrast with the results of others, which reported the opposite for similar systems.[2,4] For regimes

where no bubbles are created, self-diffusophoresis and self-electrophoresis were reported.[5,6] Other colloidal particle structures, that rely on jet like propulsion[7,8] have been described based on bubble motion theory. The experimental data was however not modeled or simulated until now.[9,10]

Janus plate motors as described in our publication are in principle, nothing new; Whitesides introduced Janus plate based motor systems in 2002.[11] The differences between his system and ours are, that our motors are spherical, 100-200x smaller than his[11] and exhibit a Janus structure on the flat areas. Whitesides' plates were half-moon like and had a hydrophobic patch on the outer rim, leading to dynamic self-assembly structures.[11]

The motion speed of bubble propelled particles was described to be in the direction of the catalyst for diffusophoresis whereby it is away from the catalyst in case of bubble propulsion mechanism.[12] Gibbs described the bubble propelled colloidal motion speed to be related to Langmuir equation whereby the speed is linearly related to the fuel and exponentially to the surface energy of a Janus particle, see equation S1.[12]

$$v \propto \gamma \frac{k\alpha c}{1 + ac} \qquad \text{(S1)}$$

Here, v represents the particle speed, γ the surface tension, α is the Langmuir adsorption constant, c the concentration and k the equilibrium constant. It is also worthy to note, that different motion mechanisms exhibit different speed relations to the surface tension.[12] Electrophoresis was not modelled to the surface tension at all while diffusophoresis shows a linear correlation.[12]

The Schmidt group reported that the Pt inside their tubes only wets when surfactants decreased the surface tension, so that water and H_2O_2 penetrated their tubes.[13] Depending on the H_2O_2 concentration, the bubble propulsion frequency ranged from 8 to 38 Hz, whereby the motion was for each step around the diameter of the bubble.[13] The motion was described by following equation:

$$v = r \times f \tag{S2}$$

with v being the speed of the particle, r the bubble radius and f the bubble production frequency.

The Zhao group used analytical equations to explain the motion within one bubble development cycle for bubble propelled Janus catalytic micromotors.[14] Their mathematical determination for particle speeds was equation S3. Their particles were driven by up to 73µm imploding bubbles and caused a oscillatory particle motion:[14]

$$v = v_0 e^{-k(A\sqrt{t} + t + Bt^2)} \tag{S3}$$

with $A = 2R_m/\sqrt{\pi\vartheta}$, $B = 2R\vartheta/32\lambda^3$, $k = 6\pi\eta R/m$, R being particle radius, η the viscosity, λ the vertical distance from centre of the fluid to the wall, ϑ the kinematic viscosity and t the time.[14] The same group presented a different speed related equation based on power law behaviour of the bubble growth:[14]

$$v = \left(\beta \int_0^t t^{4n-2} e^{kt} dt\right) e^{-kt} \tag{S4}$$

Gao investigated Janus capsules which assembled due to hydrophobic forces.[15] He observed that 2 opposing Janus capsules can cancel each other's propulsion forces, whereby only Brownian motion was observed to be left.[15] In his study, no mathematical explanation was shown.[15] The Schmidt's research group showed similar effects on tubular motors which were docked onto each other.[16] Depending on the docking position, the motion of both tubes was either cancelled completely or rotational motion was performed. [16] As in Gao's case, no equation was shown.[16] The focus of the study relied on so called 'infobubbles'.[16]

Another interesting study pointed out that nanobubbles can coalesce due to mechanical pressure, which might be the minimum nucleation site separation in general.[17,18] In addition, the study also reported that presence of nanobubbles can reduce drag.[17] Nanobubble nucleations are additionally able to attenuate temperature gradients[19], since the water does not touch the surface anymore. Furthermore, the surface temperature was reported to fluctuate, depending on nanobubble surface attachment or detachment.[19]

The Siedel group focussed on fitting the bubble radius in relation with time, departure type, nucleation side type and temperature.[20] They observed a de-pinning of the vapour nano-bubbles on heated surfaces.[20] While their fit showed a square root dependence of the bubble radius on time,[20] it does not take the bubble departure point into account as equation S5 shows:[20]

$$R \propto t^{0.5} \tag{S5}$$

with R being the bubble radius and t the time. The bubble volume V was fitted by this group to be for t<0.2 (equation S6) and t>0.2 (equation S7):[20]

$$V = 2t \tag{S6}$$

$$V = t^{0.6} \quad \text{(S7)}$$

The drag during motion of microparticles was calculated by Gibbs to be:[21]

$$F = -6\pi\mu a v \quad \text{(S8)}$$

Where F is the drag force, μ is the fluid dynamic viscosity of the solution, v the particle speed and α the sphere radius. The friction was described by:

$$F_S = F_0(F_0F_1)\frac{f - f_0}{f_1 - f} \quad \text{(S9)}$$

Here F_s represents the frictional force, with f_1 being the minimum and f_2 being the maximum produced force. The attainable forces are F_1 and F_0 for their maximum and minimum values.[21] Torques were calculated by a similar equation that did not involve the use of the attainable forces.[21] Brownian motion was simulated by Langevin approach.[21]

Solovev used the same equation as Gibbs to calculate his particles frictional motion (equation S8).[22] He got different bubble production rates for different H_2O_2 concentrations.[22] Below 5% hydrogen peroxide, his particles' bubble production rate was 8 Hz, while it was 32 Hz for >5%.[22] The speed was reported to be limited by the surfactant coverage of the catalyst, as well as by the interface tension and solution mixture.[22] Solovev also reported a corkscrew motion for 600nm asymmetric tube-like particles in 10% surfactant and 20% H_2O_2 solution.[23] These particles were able to drill into cancer cells[23], their recorded bubble production frequency was 10 Hz.[23]

Certain solvents were reported to stop the motion of catalytically driven microparticles.[24] These were DMSO, as well as sulphur containing ions and some proteins.[24] In addition, the chemotaxis of enzymes and enzyme linked particles was claimed to be directed towards substrates and

alkaline rich regions.[25] Since some cancer cells are able to produce H_2O_2 due to a distorted metabolism, Janus capsules were able to target tumour cells in 0.05% H_2O_2.[25] Similar results were reported by the Wang group, which showed that polymer tubes were able to run in blood and serum unlike CuPt tubes.[26] Also, the negative effect of commonly added surfactants on cell viability were pointed out. The tubes in this study were reported to exhibit bubble production efficiency of up to 75%, whereby the production frequency was not discussed.[26]

The bubble tail of microtubes was observed to affect the mixing of passive tracer particles in a solution while[27] the tracer displacement was explained to be fuel concentration and bubble frequency dependent. However, there was no equation on the speed fitting of the motors shown.[27]

Recently, novel ultrasound driven micro-bullets with a speed up to 100x faster than common nanoparticles were introduced.[28] Unfortunately, the properties of these micro-bullets have been scarcely investigated up to now.

Methods and Materials:

The plates were prepared by microcontact printing of polyelectrolyte multilayer (PEM) thin films according to reference [29]. First, a PEM thin film was assembled onto flat silicone rubber sheets (PDMS) via the so called layer by layer spraying deposition method.[30] The used PDMS was Sylgard 184 (Dow Corning, Midland, USA), whereby the base and curing agent were mixed at a ratio of 10:1, degassed in vacuum for 30 minutes and cured at 70°C for 3 hours. Then, the PDMS-air interface was used for PEM assembly. The spraying time for each polyelectrolyte solution and the rinsing water were 6 seconds. The used spraying cans were DC

(Dünnschichtchromatographie Sprühflaschen) (Carl Roth, Karlsruhe, Germany). In total, 6 bilayers of the PEM were assembled onto the PDMS.

The PEM was assembled from polyacrylacetate (PAA) (1800 g/mol) and polyallylamine hydrochloride (PAH) (56000g/mol), which were both purchased from Sigma, St. Luis, USA. The polyelectrolytes were dissolved at concentrations of 1 g/L using 0.5 Mol/L NaCl in ultrapure water (18.6 MΩ·cm, Elga Labwater, Beijing, China). After assembling the PEM (6 bilayers of PAA and PAH with PAH being the terminating layer) onto a flat silicone PDMS sheet, a structured silicon chip was pressed in aqueous conditions with a pressure of 20 g/cm^2 for 30 seconds onto the PEM coated PDMS. This process creates structured PEM plates. Subsequently these PEM plates were transferred to a PVA (polyvinylalcohole) coated glass substrate via microcontact printing by pressing the PEM coated PDMS at a pressure of 20 g/cm^2 for 30 seconds onto the PVA coated glass slides (30% relative humidity, 20 °C). The PEM on the PVA was first sputtered with 30-45nm of platinum (Pt) and then the PVA was dissolved in hot water. Please note, that instead of using flat PDMS and a structured silicon chips, also a structured PDMS stamp can be used to microcontact print PEM onto substrates with higher surface energy than PDMS, as noted in the main article and reference [29]**.**

The gained anisotropic (Pt only on one side of the PEM) Pt-PEM micro-plates were then observed in an Olympus BX51 microscope with video microscopy at a frame rate of 8-10 images per second. The movement of the particles was achieved by addition of hydrogen peroxide solution (30% chemical reagents, Tianjin, China). The speed of the particles, bubble creation rate and bubble sizes were determined by video analysis using ImageJ (National Institute of Health, USA) using the particle tracker and length measurement plug-ins.

These PEM based plate motors were chosen because they offer 1 to 7 different nucleation sites on the same particle due to the line tension based particle creation, causing particles with heterogeneous rough borders (heterogeneous roughness is on the scale of hundreds of nm, the plates themselves are homogenously round on the microscale) within single production batches. This rough 2D border is valid for testing the theory outlined below.

Plate motors were investigated via Atomic force microscopes (AFM) (Dimension Fast Scan, Brucker, Billerica, USA) to determine the plate thickness and structural homogeneity. The pristine PEM plates have a thickness of 8 nm (see Figure S1) while the Pt sputtering adds another 30-45 nm in form of a particle monolayer (see Figure S1). Concerning the images featured, the AFM images were made investigating the PEM on a PDMS substrate (better force contrast). The SEM images were acquired using a Helios NanoLab 600i (FEI, Hillsboro, Oregon, USA), on plate motors printed onto a gold coated silicon wafer. As shown in Figure S1b) and d), the PEM plate motors are regular on large scale. The black and grey dots seen in the same figure are dust particles due to air pollution at the production site.

Used mathematical approach and comparison of the approach with existing methods

Although the bubble production rate is cyclic, even in the presence of ultrasound waves (where the bubble is ejected earlier)[31]; there is no mathematical description capable to consider this.[1] An additionally unsolved theoretical problem is the fact that according to current theoretical considerations, autonomous moving objects should slow down due to surfactant introduction.[32] Recent studies on the contrary show, that the speed of colloidal motors can be significantly increased due to lowering the surface energy needed to form a bubble.[4] This results in higher bubble frequencies and higher speed.[4]

The main difference of the used equations to existing models is the approach and the goal of the study. In reference [14], only isolated bubble cycles were investigated. Furthermore, the goal in reference [14] was a force (bubble pushing force) and drag estimation. The catalytical turnover rate was also not of concern here, since the oscillating motion might additionally affect this turnover rate via mass transport effects, making the system more complicated. The goal therefore, was a formalism being able to explain oscillating particle motion based on bubble radius and nucleation site alignment; it was not to develop a drag based equation, since these already exist.

Finding a relation of our system to friction and propulsion forces is easily possible by relating the determined or simulated speed to the stokes drag, similar to reference [12]. This way, the propulsion force can be calculated easily.[12,14] For propulsion effects within a single cycle, we refer to reference [14].

The fitting formula is based mainly on the experimental conditions influencing the system rather than being of pure analytical nature. Below are the equations used for fitting speed, bubble radius and factor k_{bf}:

$$V = B + \frac{C}{C_0} k_b sin\left(f \frac{C}{C_0} k_{bf} t\right) \quad \text{(S10)}$$

$$k_{bf} \approx \frac{1}{\gamma_s K} \quad \text{(S11)}$$

$$R = B + k_b R_{max} sin\left(f \frac{C}{C_0} k_{bf} t\right) \quad \text{(S12)}$$

The main reason for using a sine function in (S10) and (S12) is due to the fact that the bubble development occurs in a cyclical fashion with a more or less regular frequency. Until now, such an effect was not modelled mathematically, although frequency dependent bubble developments were pointed out regularly[16,22,23].

The speed, as well as the frequency, decrease in relation to the decreasing fuel is denoted by $\frac{C}{C_0}$ with C being the current fuel concentration and C_0 being the initial fuel concentration. Such fuel concentration dependencies were also regularly reported in literature as in the case of Solovev, who in 2010 reported a fuel dependent frequency in addition to a frequency dependent motion.[22] A report on the speed and bubble frequency dependence on temperature and H_2O_2 concentration of Janus microparticles was also recently published by the He group.[33] Interestingly enough, both publications did not show a mathematical approach to explain this decrease in speed.

In the past, the fuel dependence was described by a Langmuir like equation; however to the knowledge of the authors, no mathematical fit of experimental data was made.[12] Also, the description of dynamic systems, like a catalyst with an equation developed originally for static systems, is difficult.[12]

Since catalysts additionally depend on temperatures, we use the variable 'f' in our approach. This variable is sensitive to temperature, since increases in solvent temperature are known to increase the catalytic activity of Janus particles (e.g. horse radish catalase and platinum).[9,12] We also would like to point out, that the particle shape and speed additionally influence the catalytic turnover rate. These parameters are regarded constant in this work, since the particles were already moving at the start of our video recording (final speed and temperature already reached and no change in shape).

The constant B (denoted as half maximum speed and in case of equation 3 half bubble size) is necessary to prevent mathematical artefacts like moving backwards due to the sine function dipping into negative values when approaching π to 2π.

K_b is the surface tension to speed constant of for each produced bubble ($k_b \sim \gamma/\eta$, whereby η is the viscosity and γ the surface tension), whereas k_{bf} is the frequency dependence of the bubble surface tension with K being the efficiency constant. The need for such a parameter alignment in equation S10 (and S11) are reports from the Schmidt group, about an increased bubble production rate due to lower Poisson pressure caused by the addition of surfactant as reported in reference [34]. The constant K is related to the area of oxygen collection and diffusion into the bubbles. It could be regarded close to 1 for tubes (oxygen cannot diffuse out of tube and has to form bubbles) but much lower for flat particles since multiple diffusion directions are possible, which in turn lower the chance of an oxygen molecule ending up in the bubble. The feasibility of such a constant is obvious by comparing different bubble frequencies between similarly shaped particles (e.g. tubes, plates, spherical particles or capsules).

The sum over the forces with the motion vector is based on the description of others that the final motion of particles is proportional to each bubble radius.[13] The bubbles can push against each other or (depending on alignment) push together into the same direction and are therefore considered classical force vectors. Like classical force vectors, they can be added together or cancel each other out and are in cosine to each other as stated in reference [35]. Since the oxygen collection plays a fundamental role for the bubble growth and for the surface force gradients along the plate, the area of oxygen collection A is needed. In A, a homogenous oxygen production over the whole particle area is assumed. In this study, A was assumed to be 0.5 for 2 nucleation points. W= cos (θ) with θ being the angle between the bubbles and δ= V/R_{max}.

$$Vx,y,z = \sum_{i=0}^{n} W_{X,Y,Z} \times A \times R \times \delta \qquad \text{(S13)}$$

Comparison with existing systems and approaches:

The presented approach tries to mathematically relate the particle orientation with the particle propulsion over several bubble production cycles. The presented formulas are also different compared to previous approaches as can be seen in the review section above. Furthermore, through the use of mathematical bases, the work explains observations which were discussed but not calculated or simulated in previous literature. These parameters include the motion of the particles depending on the bubble production frequency, the bubble production rate depending on H_2O_2 concentration or the bubble life cycle stages.[13,33]

Other observations, like the final movement of a particle with 2 opposing bubbles, led to different results than for 2 isolated motors[15,16] pushing against each other, whereby the final motion observed in this study was factor 3-6 above Brownian motion, due to unequal bubble power. The observation from Bhushan that nanobubbles reduce drag, is most likely responsible for the high speed observed in our system and for the general failure of many theories.[17] Bhushan's observed separation limit and pressure induced nanobubble fusion is likely to be the minimum separation distance for the nucleation sites in our system to reliably produce oscillating bubbles.[17] Taking the Brownian motion and rotation in a semi-analytical approach into account, the motion of one particle can be calculated and forecasted more reliably than by purely analytical approaches.

Thermophoretic effects due to the Pt catalyst heating up during catalytic reactions are expected to be negligible, due to temperature shielding of the nanobubbles.[17,18] The observation that surface temperatures of self-heating substrates are fluctuating with nanobubble nucleation and de-pinning frequencies supports our approach.[19]

The k_b term is regarded in some publications to deliver an exponential contribution to the speed; in our equation, we show a linear contribution. Since the amount of data on this topic is at this point in time is very low, and exponential as well as linear relations are currently published,[12,27] we cannot rule out that for different surface energies, a k_b^2 might be required.

Effect of surface energy gradients

Surface energy gradients are only valid for an interface gradient which is regularly re-established and offers also clear nucleation points. In the case of samples with a not fixed nucleation point (as occurred in 30-60% of the microplates, depending on batch) where the system has no regular or defined surface gradient, the proposed approach is not useful. As for the case of pre-nucleation of bubbles, where smaller (sub-micrometre to micrometre) bubbles form then "roll" along the interface to merge with larger bubbles the approach was found to be not precise. In the special case of true nanobubbles, which due to the experimental demand could not be observed here, (only bubbles in the range of hundreds of nm could be observed) the system is expected to give correct results, since the used theory is an extension of Paxton's surface force theory, who observed nanobubbles in his system.[32] Different surface energies of the substrate were not studied here due to all common unmodified polyelectrolytes being hydrophilic. Literature reports, exist however of the surface tension being related exponentially with speed.[12,21] The substrate surface energy cannot be omitted, since it significantly affects the propulsion as Wang[26] showed for novel polymer based tubes that move in contrast to copper and Pt based tubes in protein containing water. These effects can be described theoretically by a modified k_b constant in equation S10-S13.

The shape of such particles also influences significantly the particle speed and motion path. This was shown by Zhao's group in terms of anisotropic autonomous moving particles featuring an corkscrew path.[12,21] Since such particles exhibit a permanent rotational motion, the forecast method only works by adding a rotational parameter into equation S13. The increased motion is easily described by equation S10 in terms of an increased B.

Effects of hydrogen peroxide concentration

Neglecting the fuel concentration changes led in the observed case (time >5 seconds) to an overestimation of the particle speed (see SI Figure S3). The decrease of speed is in line with the hydrogen peroxide or HCl concentration dependence of other colloidal motors[31] reported in literature[33]. These particles slow down and cease motion after the exhaust of their fuel.[33,36] The single bubble propelled particle motion was up to 77 μm/S, which allowed only 5 seconds to be observed continuously, since the particles left the observed area. Following the particle manually by moving the sample stage, allowed for longer observation times of the particles, which confirmed the trend of slowing motion with exhausting fuel.

In addition, single nucleation site based Janus micro particles are known to exhibit temperature dependent speed bubble production.[12,33] These effects are covered in our equation by the terms f and $\sin(C/C_0)$.

a)

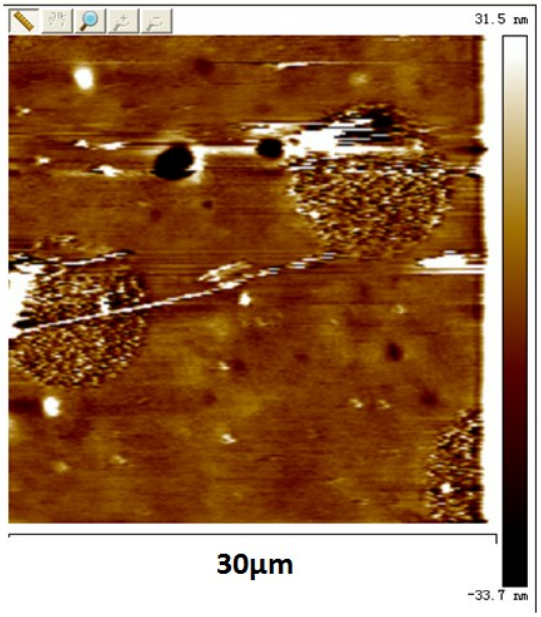
31.5 nm
30µm
-33.7 nm

b)

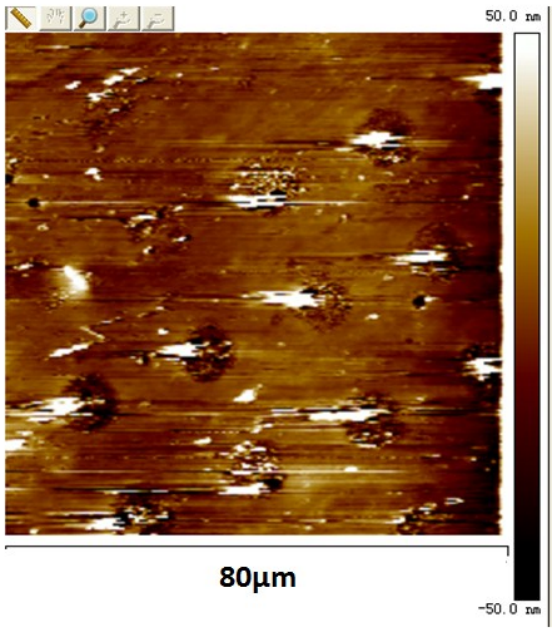
50.0 nm
80µm
-50.0 nm

c)

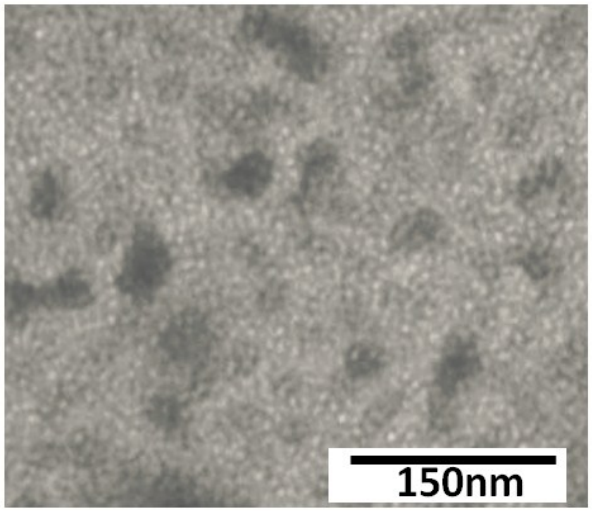
150nm

d)

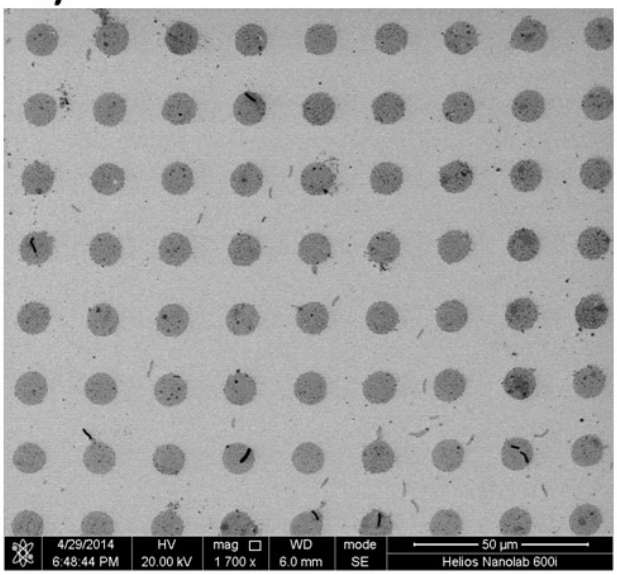
4/29/2014
6:48:44 PM
HV
20.00 kV
mag
1 700 x
WD
6.0 mm
mode
SE
50 µm
Helios Nanolab 600i

e)

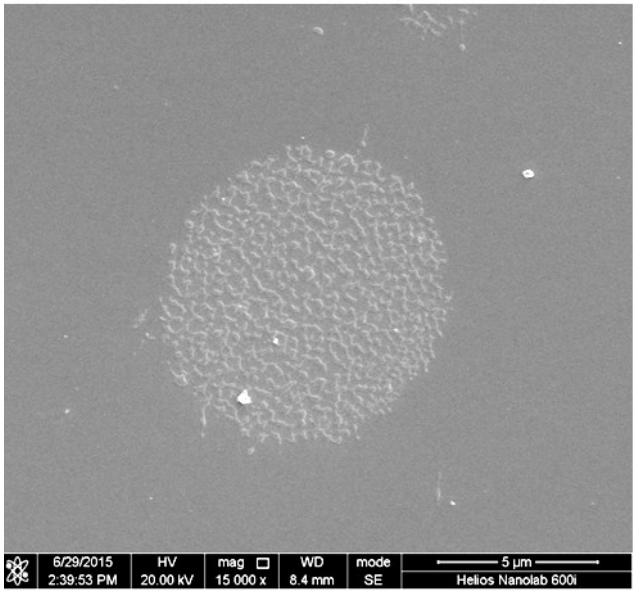

Figure S1. Characterization of the produced plate motors. a) AFM image of 2 PEM plates on PDMS; b) overview AFM image; c) TEM image zoom in of sputtered Pt nanoparticles (30-45nm diameter) on PEM microplate; d) SEM overview with gold substrate; e) SEM of a single PEM plate showing surface morphology. Please note that the positive charge terminated PEM causes the negatively charged cantilever to frequently stick to the PEM, causing hangs and white lines in the AFM image.

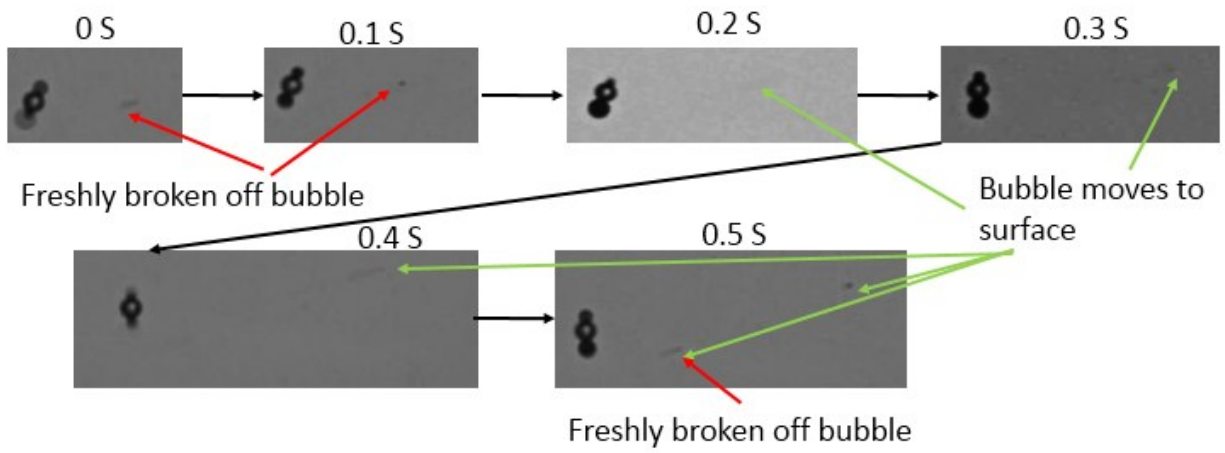

Figure S2. Time series of bubbles separated from the plate motor. The bubbles break off and move out of focus towards the air water interface. Depending on shutter position and lensing effects (due to bubble geometry), the bubble is not always clear in whole time series.

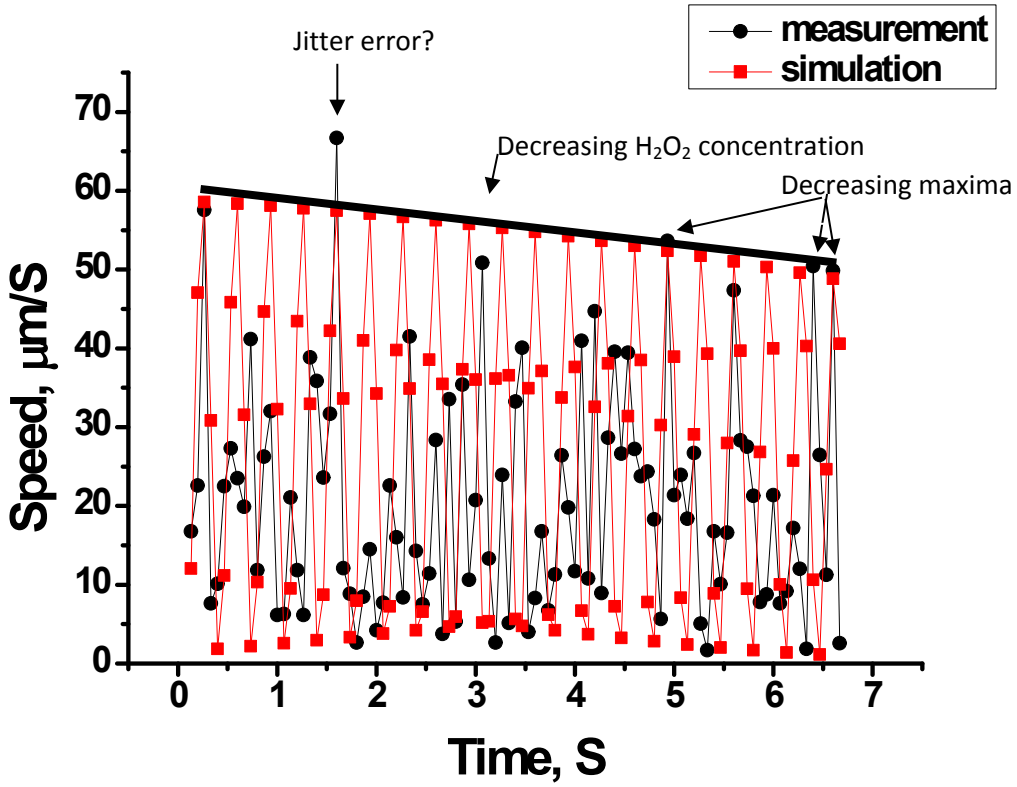

Figure S3. Development of colloidal particle speed in relation to decreasing hydrogen peroxide concentration. A decreasing hydrogen peroxide concentration causes the fit to forecast 85% of the large peaks (n=7) correctly, while it is 14% for a constant hydrogen peroxide concentration. The speed fluctuation can't be simulated 100% in accordance with the simulation due to the nucleation of sub-microbubbles which affect the surface tension close of the particle. Additionally, the slow camera does not facilitate time-stamps. For this reason, a jitter error for the fastest motion point cannot be excluded.

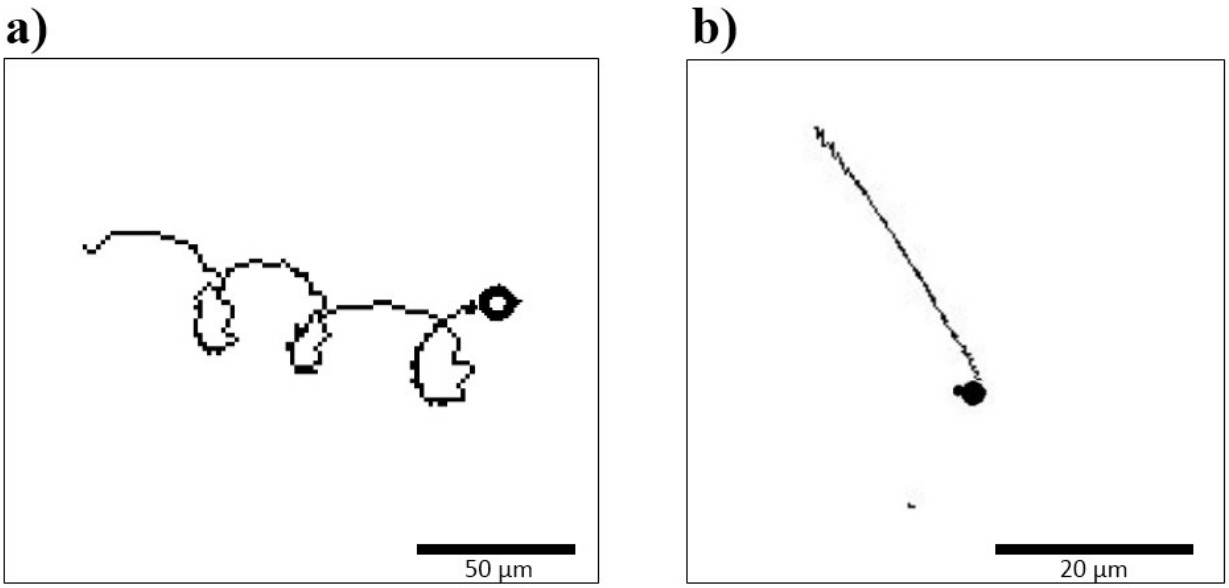

Figure S 3. Path of colloidal motor plates a) single bubble propulsion, scale bar 50µm, path travelled in 6.5S; b) propulsion with 2 bubbles on opposite sites, scale bar 20µm, path travelled in 13S.

References

1. S. Wang and N. Wu, *Langmuir*, 2014, **30**, 3477–86.

2. J. G. Gibbs and Y.-P. Zhao, *Appl. Phys. Lett.*, 2009, **94**, 163104–3.

3. Y. Wu, Z. Wu, X. Lin, Q. He, and J. Li, *ACS Nano*, 2012, **6**, 10910–10916.

4. H. Wang, G. Zhao, and M. Pumera, *J. Phys. Chem. C*, 2014, **118**, 5268−5274.

5. Y. Wang, R. M. Hernandez, D. J. Bartlett, J. M. Bingham, T. R. Kline, A. Sen, and T. E. Mallouk, *Langmuir*, 2006, **22**, 10451–6.

6. R. Golestanian, T. Liverpool, and A. Ajdari, *Phys. Rev. Lett.*, 2005, **94**, 220801.

7. G. Zhao, S. Sanchez, O. G. Schmidt, and M. Pumera, *ChemComm*, 2012, **48**, 10090–10092.

8. A. a. Solovev, S. Sanchez, M. Pumera, Y. F. Mei, and O. G. Schmidt, *Adv. Funct. Mater.*, 2010, **20**, 2430–2435.

9. J. Vicario, R. Eelkema, W. R. Browne, A. Meetsma, R. M. La Crois, and B. L. Feringa, *Chem. Commun. (Camb).*, 2005, 3936–8.

10. S. Fournier-Bidoz, A. C. Arsenault, I. Manners, and G. a Ozin, *Chem. Commun. (Camb).*, 2005, 441–3.

11. R. F. Ismagilov, A. Schwartz, N. Bowden, and G. M. Whitesides, *Angew. Chem. Int. Ed. Engl.*, 2002, **41**, 652–654.

12. J. Gibbs and Y. Zhao, *Front. Mater. Sci. China*, 2011, **5**, 25–39.

13. Y. Mei, A. Solovev, S. Sanchez, and O. G. Schmidt, *Chem. Soc. Rev.*, 2011, **40**, 2109–2119.

14. M. Manjare, B. Yang, and Y.-P. Zhao, *Phys. Rev. Lett.*, 2012, **109**, 128305.

15. W. Gao, A. Pei, X. Feng, C. Hennessy, and J. Wang, *J. Am. Chem. Soc.*, 2013, **135**, 998–1001.

16. A. Solovev, S. Sanchez, and O. G. Schmidt, *Nanoscale*, 2013, **5**, 1284–93.

17. Y. Wang, B. Bhushan, and X. Zhao, *Nanotechnology*, 2009, **20**, 045301.

18. L. Zhang and M. Shoji, *Int. J. Heat Mass Transf.*, 2003, **46**, 513–522.

19. S. Witharana, B. Phillips, S. Strobel, H. D. Kim, T. McKrell, J.-B. Chang, J. Buongiorno, K. K. Berggren, L. Che, and Y. Ding, *J. Appl. Phys.*, 2012, **112**, 064904.

20. S. Siedel, S. Cioulachtjian, and J. Bonjour, *Exp. Therm. Fluid Sci.*, 2008, **32**, 1504–1511.

21. J. G. Gibbs, S. Kothari, D. Saintillan, and Y. P. Zhao, *Nano Lett.*, 2011, **11**, 2543–2550.

22. A. a. Solovev, S. Sanchez, M. Pumera, Y. F. Mei, and O. C. Schmidt, *Adv. Funct. Mater.*, 2010, **20**, 2430–2435.

23. A. A. Solovev, W. Xi, D. H. Gracias, S. M. Harazim, C. Deneke, S. Sanchez, and O. G. Schmidt, *ACS Nano*, 2012, **6**, 1751–1756.

24. G. Zhao, S. Sanchez, O. G. Schmidt, and M. Pumera, 2013, **5**, 2909–2914.

25. F. Peng, Y. Tu, J. C. M. Van Hest, and D. A. Wilson, 2015, 1–5.

26. W. Gao, S. Sattayasamitsathit, J. Orozco, and J. Wang, *Nanoscale*, 2013, **5**, 8909–8914.

27. J. Orozco, B. Juradosa, G. Wagner, W. Gao, R. Vazquez-duhalt, S. Sattayasamitsathit, M. Galarnyk, A. Corte, D. Saintillan, and J. Wang, *Langmuir*, 2014, **30**, 5082−5087.

28. W. Gao and J. Wang, *Nanoscale*, 2014, **6**, 10486–10494.

29. M. Gai, J. Frueh, A. Girard-Egrot, S. Rebaud, B. Doumeche, and Q. He, *RSC Adv.*, 2015, **5**, 51891–51899.

30. J. B. Schlenoff, S. T. Dubas, and T. Farhat, *Langmuir*, 2000, **16**, 9968–9969.

31. T. Xu, F. Soto, W. Gao, V. Garcia-Gradilla, J. Li, X. Zhang, and J. Wang, *J. Am. Chem. Soc.*, 2014, **136**, 8552–5.

32. W. F. Paxton, K. C. Kistler, C. C. Olmeda, A. Sen, S. K. St Angelo, Y. Cao, T. E. Mallouk, P. E. Lammert, and V. H. Crespi, *J. Am. Chem. Soc.*, 2004, **126**, 13424–31.

33. M. Xuan, J. Shao, X. Lin, L. Dai, and Q. He, *Chemphyschem*, 2014, **15**, 2255–60.

34. J. Simmchen, V. Magdanz, S. Sanchez, S. Chokmaviroj, D. Ruiz-Molina, A. Baeza, and O. G. Schmidt, *RSC Adv.*, 2014, **4**, 20334.

35. L. Papula, *Mathematische Formelsammlung für Ingenieure und Naturwissenschaftler*, Vieweg+Teubner, Wiesbaden, 8th edn., 2003.

36. W. Gao, A. Uygun, and J. Wang, *J. Am. Chem. Soc.*, 2012, **134**, 897–900.